30th Annual International IEEE EMBS Conference
Vancouver, British Columbia, Canada, August 20-24, 2008

Numerical Analysis of Temperature Elevation in the Head due to Power Dissipation in a Cortical Implant

Kanber Mithat Silay, Catherine Dehollain, and Michel Declercq

Abstract— **This article presents the numerical analysis of temperature increase in the human head resulting from the power dissipation in a cortical implant. A 3–D head phantom with 22 tissue types and 0.2 mm x 0.2 mm x 2 mm resolution has been used in the simulations. The dependencies of the temperature increase on the power dissipation level, chip size, and location of the implant are investigated. Moreover, distributing power dissipation by using multiple integrated circuits in the implant is discussed. Maximum allowable total power dissipation in a cortical implant of size 2 x 2 mm^2 is found to be 4.8 mW, whereas, it is 8.4 mW for an implant with two chips of same size placed 10 mm apart.**

I. INTRODUCTION

Biomedical implants are becoming more and more popular with the development of miniature electrode arrays for recording the neural activity or stimulating the neurons of the central nervous system [1]–[3]. However, the operation of the implant inside the body gives rise to safety issues. One of the most important issues is the temperature elevation in the head resulting from the power dissipation in a cortical implant. As the functions of the implants increase with the number of recording/stimulation sites, the required power dissipation in the implants also increase. Nevertheless, the power dissipated in the device should be kept under a safe level to avoid potential hazards.

There are studies in the literature presenting the results of temperature increase in the tissues. As given in [4], 1 °C temperature increase in the whole–body results in behavioral disruption in rats and monkeys. It is also given that brain temperature higher than 40.5 °C results in heat stroke in humans. Although the former argument does not imply that 1 °C temperature increase in the brain will yield any damage, it is safer to keep 1 °C temperature increase in the brain as the maximum allowed temperature elevation, as done in [5], [6].

Numerical analysis of temperature elevation resulting from the operation of implant enables foreseeing the potential damages in advance, without any complex *in vivo* measurements. Hence, precautions can be taken by the designer during the design stage of the implant.

This work was supported by the Swiss National Funding (SNF) in the frame of the project *NEURO–IC*.

K. M. Silay is with the Institute of Electrical Engineering (IEL), Ecole Polytechnique Fédérale de Lausanne (EPFL), Switzerland. e-mail: kanbermithat.silay@epfl.ch.

C. Dehollain is with the Institute of Electrical Engineering, EPFL, Switzerland. e-mail: catherine.dehollain@epfl.ch.

M. Declercq is with the Institute of Electrical Engineering, EPFL, Switzerland. e-mail: michel.declercq@epfl.ch.

Many researchers have published articles on the thermal effects of biomedical implants. Temperature elevation in the eye and head from the operation of an implanted retinal stimulator has been studied in [7]–[10]. The authors have used finite–difference time–domain (FDTD) simulations with 2–D and 3–D head models in order to calculate the temperature increase resulting from both heat dissipation in the implant and exposure to electromagnetic (EM) fields. In another study, Ibrahim *et al.* simulated the temperature changes due to brain–machine interface operation by using FDTD method with an 18–tissue 2–D head phantom [5]. A more recent study investigated the temperature increase resulting from operation of a 3–D microelectrode implanted in the brain [6]. The authors used 3–D finite–element analysis with a simple three layer head model. Moreover, they measured the temperature elevation from the heat dissipation on the electrodes *in vivo* on a cat cortex exposed to air, with an infrared thermal camera [6].

This study presents numerical analysis of temperature increase in the head due to the operation of a cortical implant. The thermal elevation due to power dissipation is calculated by using an FDTD–based coupled EM–thermal simulation software SEMCAD X v13.2 with a detailed 3–D head phantom composed of 22 tissues. This study focuses only on the thermal effects of power dissipation in a cortical implant, as the temperature increase resulting from exposure to the EM fields is relatively small, compared to the temperature increase resulting from power dissipation [5], [8], [9]. Temperature elevations in the tissues are analyzed with different topologies by changing the power dissipation amount, chip size and location of the implant. Moreover, using implants with multiple integrated circuits for distributing the heat dissipation is also studied. To the best of authors' knowledge, this is the first study including numerical analysis of temperature increase in the human head due to operation of a cortical implant, with a 3–D high–detail head phantom.

II. COMPUTATIONAL METHOD

The thermal simulations used in this study are based on the Pennes bio–heat equation [11], which is widely used in literature [5]–[10], [12] for simulating temperature distribution in living tissues and which can be written as [10]:

$$\rho C \frac{\partial T}{\partial t} = \nabla \cdot (K \nabla T) + A_0 + P_d - B_0 (T - T_b) \left[\frac{\mathrm{W}}{\mathrm{m}^3} \right] \quad (1)$$

where, ρ is the tissue density [kg/m^3], C is the specific heat [J/(kg °C)], T is the temperature [°C], K is the thermal conductivity [W/(m °C)], A_0 is the basal metabolic rate [W/m^3],

P_d is the density of power dissipated in the implanted electronics [W/m^3], B_0 is the blood perfusion coefficient [W/(m^3 °C)], and T_b is the temperature of the blood [°C]. The boundary condition for the differential equation (1) at the air–skin interface is:

$$K\frac{\partial T}{\partial n} = -H_a\left(T - T_a\right)\left[\frac{\text{W}}{\text{m}^2}\right] \quad (2)$$

where, n is the normal vector to the skin surface, H_a is the convective transfer coefficient [W/(m^2 °C)] and T_a is the ambient temperature [°C].

Since we are interested in the temperature increase due to the operation of the implant, there is no need to calculate the steady–state temperature distribution, if the coefficients in (1) and (2) are constant with respect to temperature. As the safety regulations require that the maximum temperature increase in the tissues should be less than 1 °C, the material properties of tissues can be assumed to be constant for such small change of temperature. Moreover, it has been shown that the thermoregulatory behavior of the tissues is negligible compared to the temperature elevation due to implant operation [9]. By using this assumption and replacing T in (1) and (2) with $T_{ss} + T_{incr}$, which are the steady–state and incremental temperatures, respectively; the incremental bio–heat equation and the corresponding boundary condition can be found as:

$$\rho C\frac{\partial T_{incr}}{\partial t} = \nabla\cdot\left(K\nabla T_{incr}\right) + P_d - B_0 T_{incr} \quad (3)$$

$$K\frac{\partial T_{incr}}{\partial n} = -H_a T_{incr} \quad (4)$$

Incremental bio–heat equation given in (3) and (4) has been used in all of the simulations presented in this study.

III. Simulation Setup

A. Human Head Phantom

For thermal simulations, European male head phantom (EM–1 [13]) has been used, which is a 3–D phantom with 22 different tissues and is generated from the "Visible Human Project" [14]. The resolution of the head phantom in x, y, and z–axes are 0.2 mm, 0.2 mm, and 2 mm, respectively. The phantom is divided into voxels with a non–uniform grid with minimum step size of 0.25 mm in all directions.

The phantom has been truncated down to 4 cm from the top of the head in order to decrease the computational time. The discrepancy of the simulation result with the truncated phantom is 3 orders of magnitude smaller than the peak temperature increase; therefore, truncated head phantom is used in all of the thermal simulations presented in this article.

B. Material Parameters of Tissues

As the phantom was truncated to decrease the computation time, the number of tissues voxeled for the simulations decreased to 9. The thermal parameters used in (3) and (4) are collected from [7], [12], [15]. Table I presents the thermal parameters of the tissues used in the thermal simulations. For the boundary condition, the convective transfer coefficient (H_a) is chosen to be 8.3 W/(m^2 °C) [12].

TABLE I
Thermal Parameters of the Tissues Used in the Thermal Simulations [7], [12], [15].

Tissue	ρ kg/m^3	C J/(kg °C)	K W/(m °C)	B_0 W/(m^3 °C)
Blood	1060	3840	0.53	$7.19 \cdot 10^5$ [a]
Bone Marrow	1027	2700	0.22	32000
Cerebrospinal fld.	1007	4200	0.62	0
Connective tissue	920[b]	2947[c]	0.346[c]	2350[c]
Cortical bone	1990	1300	0.4	3400
Grey matter	1039	3680	0.565	40000
Skin	1100	3500	0.42	9100
Subcutis[b]	920	2500	0.25	1700
White matter	1043	3600	0.503	40000

[a]Obtained from SEMCAD X material database. Chosen in order to model the effective cooling mechanism of blood.
[b]Not available. Modeled as fat.
[c]Obtained from SEMCAD X material database.

TABLE II
Thermal Parameters of the Materials in the Implant [16].

Material	ρ kg/m^3	C J/(kg °C)	K W/(m °C)	B_0 W/(m^3 °C)
Silicon	2330	705	148	0
Copper	8960	385	401	0

C. Cortical Implant

The overall shape, size, and composition of the device depend on the application that the implant is going to be used. Since these parameters are variable, the implant is modeled with a silicon rectangular prism.

As the temperature increase resulting from fixed power consumption will be smaller for an implant occupying larger area, the default size of the implant is chosen to be 2 x 2 x 0.5 mm^3, which is small enough to be assumed as the worst case for temperature increase, when compared with the devices published previously [1]–[3].

Copper is also used in some of the simulations to model wiring. Table II shows the thermal parameters of the materials in the implant [16].

The location of the implant also depends on the application and therefore, its exact position is unknown. The default position for the implant in this study is chosen to be at the right lobe of the brain, where the uppermost layer of the grey matter is included. Fig. 1 shows the 3–D head phantom from the front view and the left view. The black line in Fig. 1(a) represents the voxeled slice including the center of the implant. Fig. 2 displays the close–up cross–section from the right lobe of the brain [see Fig. 1(b)] including the implant orientation, tissue types, and reference definitions.

For the sake of simple modeling, a reference x–y plane has been chosen at the interface between the uppermost layer of the grey matter and other tissues. For the cross–section shown in Fig. 2, this plane is at $z = -z_{ref} = -20$ mm. Moreover, a reference point is defined at the center of the bottom plane of the implant. The normal distance from the reference point to the reference plane is defined as the *depth (d)* of the implant, which is a measure of the distance of the

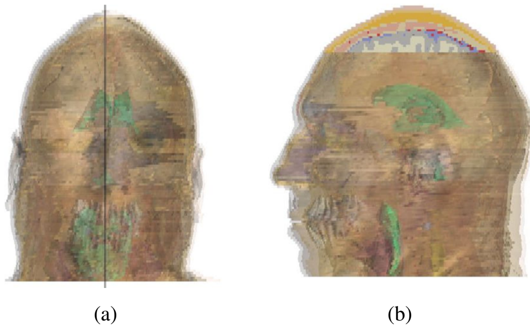

Fig. 1. 3–D human head phantom from (a) the front view, (b) from the left view, including the slice (marked in (a) with a black line) with the voxeled region at the top.

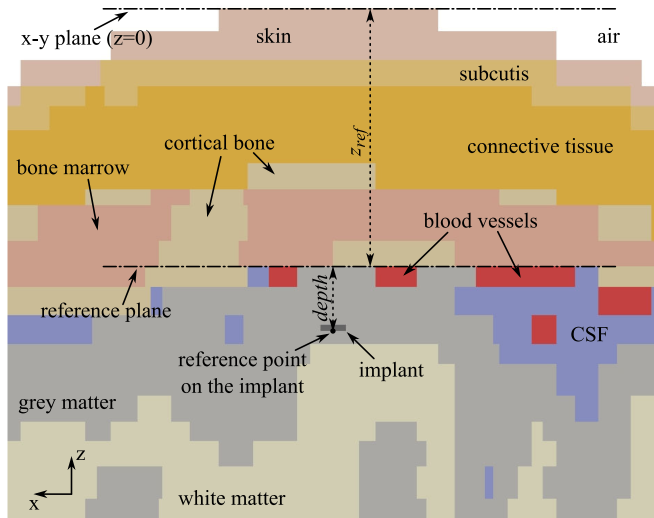

Fig. 2. Close–up cross–section from the right lobe of the brain where the implant is located.

implant to the interface. If *depth* is zero, the bottom plane of the implant is at the interface of the grey matter (default position). If it is positive, the implant is above the reference plane, or vice versa.

D. Simulation Settings

The thermal simulations in this study are run for at least 500 seconds (simulation time) to guarantee steady–state after the implant is powered. In the simulations, conformal voxels are used in order to avoid overestimation resulting from staircasing in FDTD method [17].

IV. Distributing Power Dissipation with a Multi–IC Cortical Implant

Generally, biomedical implants are powered with inductive links in order to avoid transcutaneous wires or implantable batteries [18], [19]. In order to deliver the power to the implant with high efficiency, the receiving coil should be as close as possible to the transmitting coil outside. Therefore, it is desired to place the coil between the skin and cortical bone. On the other hand, the low–noise amplifiers for detecting neural signals should be at the close proximity of the electrodes for better signal detection. Therefore, the readout circuitry should be under the cortical bone.

The implant can be designed to have multiple integrated circuits (IC) so that both high efficiency power transfer and high quality neural signal detection can be achieved. The chip above the cortical bone can be used for power/data transfer in uplink/downlink mode (transceiver IC), whereas, the chip below the cortical bone can be used for signal detection and digitization (readout IC).

Separating the tasks of the implant into multi–ICs will not only increase the performance of the system, but will also help the thermal elevation issue resulting from the operation, without increasing the size of the IC at the interface of the brain. It can be used either to relax the maximum total power dissipation allowed or to decrease the temperature elevation for fixed total power dissipation at the implant.

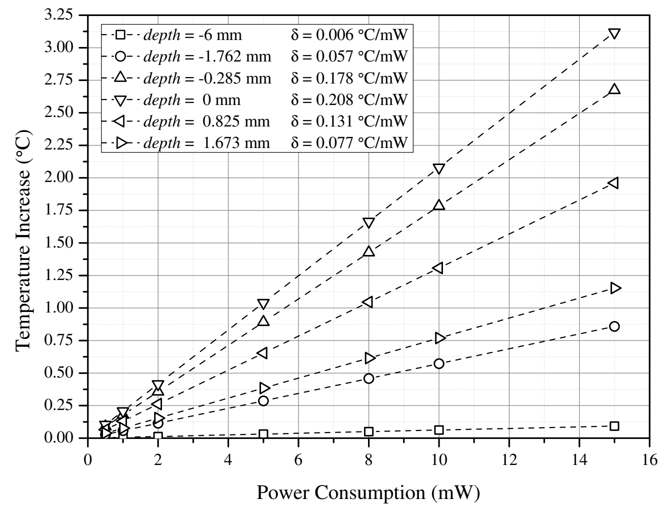

Fig. 3. Temperature increase at different depths in the phantom vs. power consumption at an implant located at $depth = 0$ mm.

V. Results

A. Temperature Increase vs. Power Dissipation

The temperature elevation in the tissues due to power dissipation at the implant was analyzed by applying different levels of heat generation rates at the implant located at the default position (i.e. $depth = 0$ mm). Fig. 3 shows the temperature increase at different depths in the phantom vs. power consumption at an implant located at $depth = 0$ mm. The δ factors given in the legend of the graph are the temperature–power slopes, which is a measure that can be used to calculate temperature increase at a location from the power consumption at the implant.[1]

B. Location of the Implant

The location of the implant is shifted in the z–axis in order to see the dependence of the temperature increase distribution with respect to *depth*. Fig. 4 displays the distribution of the

[1] δ factors are valid as long as coefficients in (3) and (4) are constant for small temperature changes.

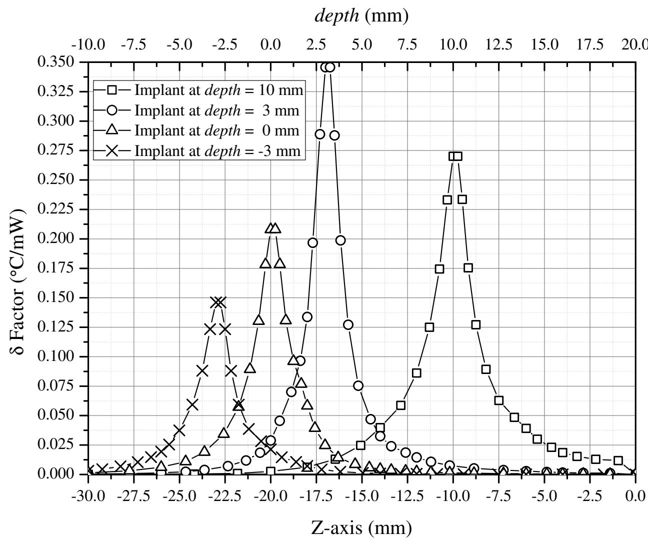

Fig. 4. Distribution of the δ factor in the z–axis for implant located at four different points.

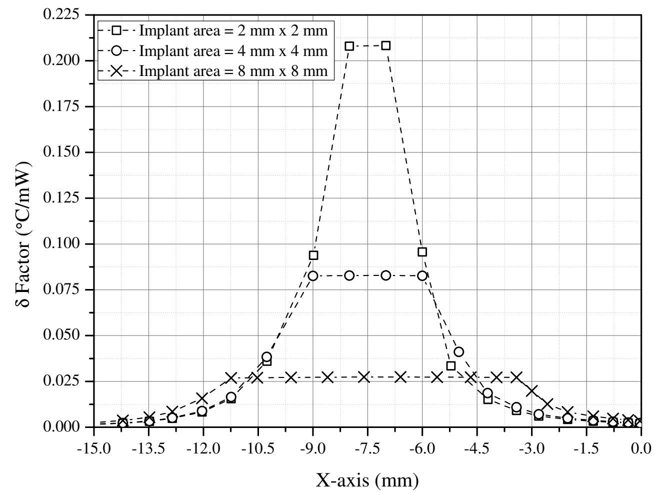

Fig. 5. Distribution of the δ factor in the x–axis for different sized implants located at $depth = 0$ mm.

δ factor in the z–axis for implant located at four different points. From these results, the peak δ factors are found to be 0.270, 0.346, 0.208, and 0.146 °C/mW for implant located at 10, 3, 0, and -3 mm, respectively.

The peak temperature increase for implant at $depth = 3$ mm (inside bone marrow) is larger than the implant located at $depth = 10$ mm (inside connective tissue). From this, one can conclude that heat transfer via thermal conduction is more effective than heat transfer with blood perfusion [see Table I].

C. Size of the Implant

In order to see the effect of the implant's size on the δ factor, three different cases are compared by setting the area of the implant to 4 mm^2, 16 mm^2, and 64 mm^2, all in square shape, while maintaining the thickness of the implant at 0.5 mm. Fig. 5 shows the distribution of the δ factor in the x–axis for different sized implants located at $depth = 0$ mm.[2] The peak δ factors obtained from these simulation results are 0.208, 0.083, and 0.027 °C/mW for the implants sized 2 x 2, 4 x 4, and 8 x 8 mm^2, respectively. It can be seen that temperature increase is a strong function of the size of the implant because the larger the surface area of the implant, the easier to dissipate the heat generated.

D. Temperature Increase in the Left Lobe

The location of the implant is moved from the right lobe to the uppermost layer of the grey matter in left lobe. The reference plane is 24 mm away from the x–y plane (i.e., $z_{ref} = 24$ mm), but the skin is also 4 mm below the x–y plane. Hence, the distance between the uppermost skin layer and the reference plane is 20 mm as the previous case. Fig. 6 shows the location of the implant in the left lobe of the brain.

The thermal simulation is done for an implant located at $depth = 0$ mm in the second reference plane on the left lobe of the brain. The peak δ factor is found to be 0.138 °C/mW, which is quite smaller than the previous location. Comparing Fig. 2 and Fig. 6(c), the reason for this decrease is found to be due to the fact that, the phantom contains cerebrospinal fluid (CSF), which has high thermal conductivity, at the interface of the brain for this situation [see Fig. 6(c)], which was not the case for the default position [see Fig. 2]. As a result, the previous case, in which the implant is at its default position, can be taken as the worst case since the location of the implant depends on the application.

E. Multi–IC Implant

A simple case of the multi–IC implant is also investigated in this study. Two silicon chips are implanted to the phantom. The readout IC is located to the default position ($depth = 0$ mm), whereas the transceiver IC is located to 10 mm above the reference plane ($depth = 10$ mm).

The simulations for multi–IC implant are done in two steps. First, in order to see the effect of presence of another chip on the temperature distribution while the other chip is dissipating power, each chip is powered individually while the other one is passive. Then, both of the chips are powered simultaneously. Fig. 7 shows the distribution of the δ factor in the z–axis for multi–IC implant. The upper graph displays the distribution while the chips are individually active, whereas, the lower graph displays the distribution while both are active simultaneously.

The peak δ factors while the chips are individually active are found to be 0.208 and 0.270 °C/mW for the readout and transceiver ICs, respectively. Comparing these results with Fig. 4, where there is only one chip implanted at a time, it can be seen that the presence of a passive silicon chip 10 mm away from the active integrated circuit results in a

[2]Note that the 2 x 2 mm^2 implant seems to occupy 1 mm in the x–axis. This is due to the fact that SEMCAD X assigns the temperature to the lowest value occupied by a voxel, i.e., the voxel lying from -8 mm to -7 mm is assigned to -8 mm point.

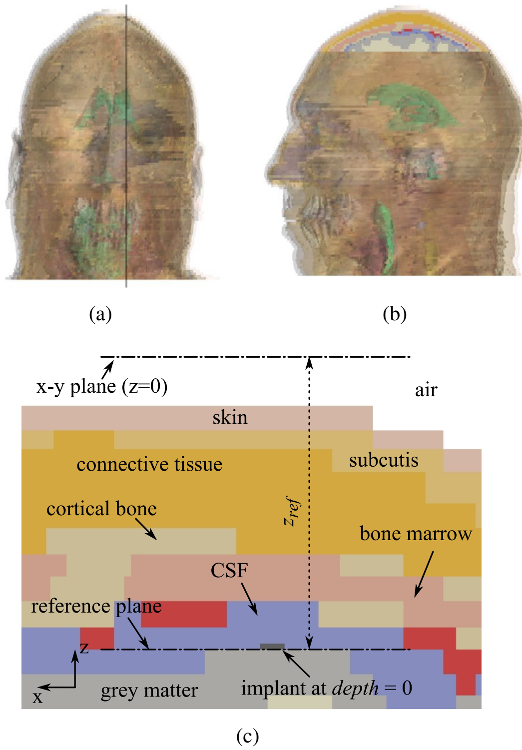

Fig. 6. Location of the implant in the left lobe of the brain from (a) the front view, (b) from the left view, (c) close–up cross–sectional view.

discrepancy less than 0.2% of the peak temperature increase.

The lower graph in Fig. 7 shows that the temperature increase at a point is the sum of the temperature increases caused by each individual IC. Therefore, one can calculate the total temperature increase at a point by adding up the temperature increase from each chip. The total temperature increase at a point is:

$$T_{incr}\left(d\right) = \delta_1\left(d\right)P_1 + \delta_2\left(d\right)P_2 + \cdots \quad (5)$$

where, d is the $depth$ of the location where T_{incr} is calculated, and P is the power dissipated in the integrated circuit.

A more important conclusion from the results given in Fig. 7 is that the power dissipation in the transceiver IC has a δ factor of only 0.0016 °C/mW at the readout IC. This value is much less than the temperature increase caused by the readout IC at that location. This result verifies that it is possible to increase the maximum allowable total power dissipation in the implant by using multiple ICs without violating the safety regulations and damaging the tissues. For example, the maximum allowable power dissipation in the implant at $depth = 0$ mm for single chip implementation is approximately 4.8 mW. If an implant with two chips is used as in this case, it is possible to dissipate 4.75 mW and 3.65 mW in readout and transceiver ICs, without increasing the temperature at any location by more than 1 °C. Fig. 8 shows the calculated temperature increase from (5) due to operation of an implant with a readout IC located at $depth = 0$ dissipating 4.75 mW and a transceiver IC located at $depth = 10$ dissipating 3.65 mW.

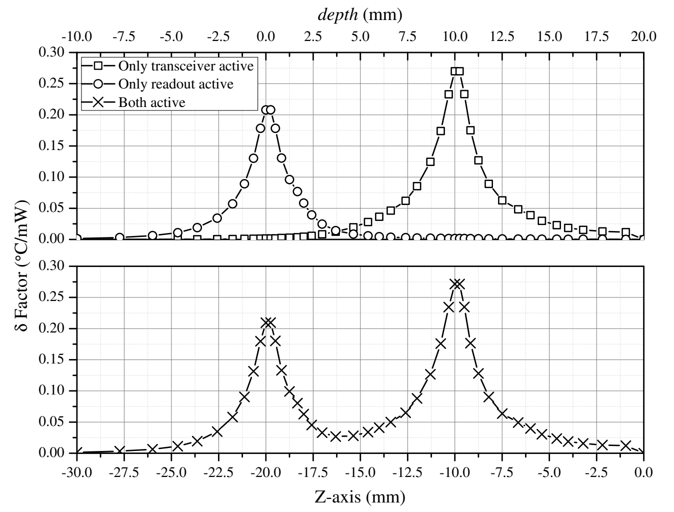

Fig. 7. Distribution of the δ factor in the z–axis for multi–IC implant.

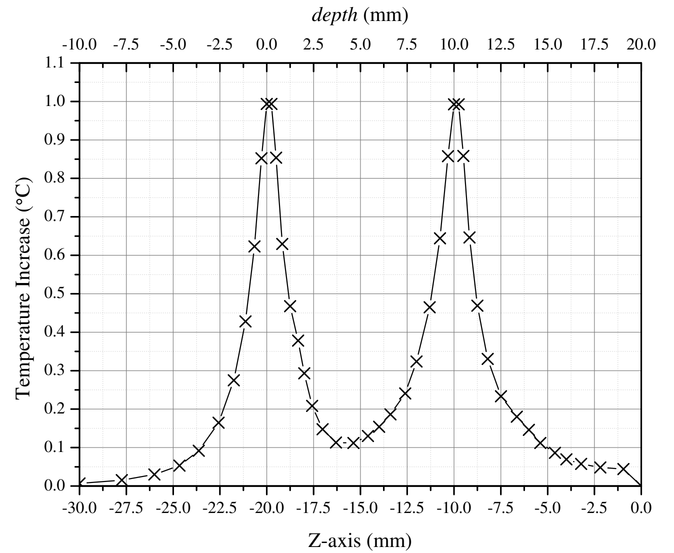

Fig. 8. Calculated temperature increase due to operation of an implant with readout and transceiver ICs dissipating 4.75 mW and 3.65 mW, respectively.

F. Multi–IC Implant with a Copper Wire

As there will be wiring between the integrated circuits of the multi–IC implant, there will be heat conduction through the wires, and its effect must be taken into account. A copper block of 0.5 x 0.5 x 9.5 mm^3 is added between the chips in order to model a simple wiring.

Fig. 9 displays the temperature increase distribution in the x and z–axes resulting from power dissipation of 1 mW in each IC. Maximum temperature rise is calculated to be 0.1763 °C for 1 mW power dissipation in each chip. It can be seen that maximum temperature increase is decreased compared to the previous case where there was no wiring, because of the fact that copper's thermal conductivity is very high and the wire increases the surface area for dissipation of the heat generated in the ICs.

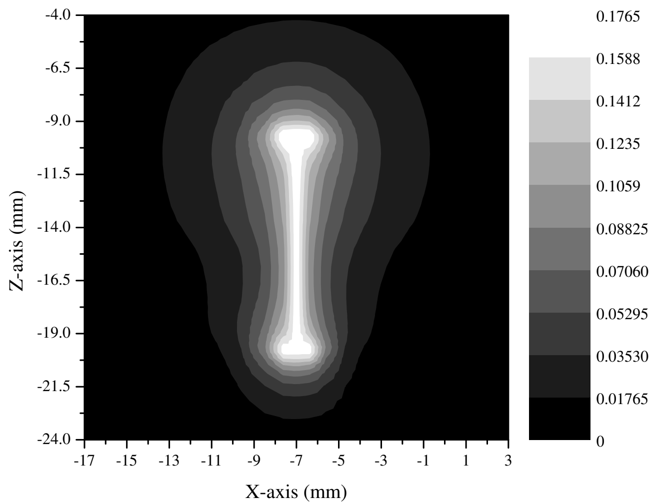

Fig. 9. Temperature increase distribution in the x and z–axes resulting from power dissipation of 1 mW in each IC.

VI. Conclusion

In this paper, a comprehensive study of thermal elevation in the head due to power dissipation in a cortical implant is presented. This paper focuses on the temperature increase resulting from the power dissipation in the implant because the thermal elevation due to EM fields is relatively small with respect to the elevation due to power dissipation.

The temperature increase is simulated in a 3–D human head phantom composed of 22 tissues and having 0.2 x 0.2 x 2 mm^3 resolution, by using an FDTD–based simulation software. The phantom is truncated down to 4 cm in order to decrease the simulation time without sacrificing the accuracy of the results. As the phantom is truncated, the number of tissues included in the simulations decreased to 9. The cortical implant is modeled as a silicon rectangular prism of size 2 x 2 x 0.5 mm^3 and is placed to the uppermost layer of the grey matter tissue in the right lobe of the brain.

The temperature elevation from the power dissipation in the implant is analyzed by monitoring the temperature increase at different locations. Additionally, the dependency of thermal elevation on the location and size of the implant are also investigated.

Distribution of the power dissipation in an implant by using multiple integrated circuits is discussed. It has been shown that having multiple ICs in a cortical implant will not only help increasing the performance of the system, but will also help distributing the heat generated. From the simulation results, the maximum allowable total power dissipation in the implant is calculated to be 8.4 mW, whereas, it is 4.8 mW for single–chip configuration. Moreover, the effects of connecting a wire between the chips are also considered by adding a copper block. It is found that the heat is more effectively distributed because copper has high thermal conductivity and it increases the surface area for heat dissipation.

It is expected that the temperature increase will drop with the use of cortical recording electrodes, as they will increase the surface area. The results of this study can be taken as the worst case limitations for the operation of a cortical implant.

The packaging of the implant is also another issue that should be taken into account in thermal simulations and it is currently under study.

Acknowledgements

The authors gratefully acknowledge Schmid & Partner Engineering AG for their help and support for SEMCAD X.

References

[1] K. D. Wise, D. J. Anderson, J. F. Hetke, D. R. Kipke, and K. Najafi, "Wireless implantable microsystems: High–density electronic interfaces to the nervous system," *Proc. IEEE*, vol. 92, no. 1, pp. 76–97, 2004.

[2] R. R. Harrison, P. T. Watkins, R. J. Kier, R. O. Lovejoy, D. J. Black, B. Greger, and F. Solzbacher, "A low–power integrated circuit for a wireless 100–electrode neural recording system," *IEEE J. Solid-State Circuits*, vol. 42, no. 1, pp. 123–133, 2007.

[3] S. O'Driscoll, T. Meng, K. Shenoy, and C. Kemere, "Neurons to silicon: Implantable prosthesis processor," in *Proc. Int. IEEE Solid–State Circuits Conf. (ISSCC) 2006*, 2006, pp. 2248–2257.

[4] *IEEE standard for safety levels with respect to human exposure to radio frequency electromagnetic fields, 3 kHz to 300 GHz*, IEEE Std. C95.1-2005, 2006.

[5] T. S. Ibrahim, D. Abraham, and R. L. Rennaker, "Electromagnetic power absorption and temperature changes due to brain machine interface operation," *Ann. Biomed. Eng.*, vol. 35, no. 5, pp. 825–834, 2007.

[6] S. Kim, P. Tathireddy, R. Normann, and F. Solzbacher, "Thermal impact of an active 3–D microelectrode array implanted in the brain," *IEEE Trans. Neural Syst. Rehab. Eng.*, vol. 15, no. 4, pp. 493–501, 2007.

[7] S. C. DeMarco, G. Lazzi, W. T. Liu, J. D. Weiland, and M. S. Humayun, "Computed SAR and thermal elevation in a 0.25–mm 2–D model of the human eye and head in response to an implanted retinal stimulator – Part I: Models and methods," *IEEE Trans. Antennas Propagat.*, vol. 51, no. 9, pp. 2274–2285, 2003.

[8] G. Lazzi, S. C. DeMarco, W. T. Liu, J. D. Weiland, and M. S. Humayun, "Computed SAR and thermal elevation in a 0.25–mm 2–D model of the human eye and head in response to an implanted retinal stimulator – Part II: Results," *IEEE Trans. Antennas Propagat.*, vol. 51, no. 9, pp. 2286–2295, 2003.

[9] K. Gosalia, J. Weiland, M. Humayun, and G. Lazzi, "Thermal elevation in the human eye and head due to the operation of a retinal prosthesis," *IEEE Trans. Biomed. Eng.*, vol. 51, no. 8, pp. 1469–1477, 2004.

[10] G. Lazzi, "Thermal effects of bioimplants," *IEEE Eng. Med. Biol. Mag.*, vol. 24, no. 5, pp. 75–81, 2005.

[11] H. H. Pennes, "Analysis of tissue and arterial blood temperatures in the resting human forearm," *J. Appl. Physiol.*, vol. 1, no. 2, pp. 93–122, 1948.

[12] P. Bernardi, M. Cavagnaro, S. Pisa, and E. Piuzzi, "Specific absorption rate and temperature elevation in a subject exposed in the far–field of radio–frequency sources operating in the 10–900-MHz range," *IEEE Trans. Biomed. Eng.*, vol. 50, no. 3, pp. 295–304, 2003.

[13] Schmid & Partner Engineering AG. (2008) SEMCAD X Homepage. [Online]. Available: http://www.semcad.com/simulation/

[14] National Library of Medicine, USA. (2007) The Visible Human Project. [Online]. Available: http://www.nlm.nih.gov/research/visible/

[15] F. A. Duck, *Physical Properties of Tissue: A Comprehensive Reference Book*. San Diego, CA: Academic, 1990.

[16] (2008) Engineering Fundamentals Online Database. [Online]. Available: http://www.efunda.com/materials/elements/

[17] *SEMCAD X Reference Manual*, Schmid & Partner Engineering AG, Sept. 2007.

[18] M. Sawan, Y. Hu, and J. Coulombe, "Wireless smart implants dedicated to multichannel monitoring and microstimulation," *IEEE Circuits Syst. Mag.*, vol. 5, no. 1, pp. 21–39, 2005.

[19] K. M. Silay, C. Dehollain, and M. Declercq, "Improvement of power efficiency of inductive links for implantable devices," in *Proc. PRIME'08 Conf.*, 2008, pp. 229–232.